Opportunities to monitor the urban atmospheric turbulence using unmanned aerial system

Shelekhov, Alexander, Afanasiev, Alexey, Kobzev, Alexey, Shelekhova, Evgenia

Alexander P. Shelekhov, Alexey L. Afanasiev, Alexey A. Kobzev, Evgenia A. Shelekhova, "Opportunities to monitor the urban atmospheric turbulence using unmanned aerial system," Proc. SPIE 11535, Remote Sensing Technologies and Applications in Urban Environments V, 1153506 (20 September 2020); doi: 10.1117/12.2573486

SPIE.

Event: SPIE Remote Sensing, 2020, Online Only

Opportunities to monitor an urban atmospheric turbulence using unmanned aerial system

Alexander P. Shelekhov[a*], Aleksey L. Afanasiev[b], Alexey A. Kobzev[a], Evgenia A. Shelekhova[a]
[a]Institute of Monitoring of Climatic and Ecological Systems SB RAS, 10/3, Academichesky Ave, 634055, Tomsk, [b]V.E. Zuev Institute of Atmospheric Optics Organization SB RAS, 634055, Tomsk, Russia, 1, Academician Zuev square

ABSTRACT

The problem of ideal hover of an unmanned aerial vehicle in a turbulent atmosphere is considered, and the equations for estimation of turbulent fluctuations of the longitudinal and transverse components of horizontal winds are derived independently of the unmanned aerial vehicle orientation and wind direction. Experiments were carried out on the territory of the Geophysical observatory of Institute of Monitoring of Climatic and Ecological Systems, Siberian Branch, Russian Academy of Sciences. It is situated in Tomsk Akademgorodok, on the territory with complex orography, in a parkland zone with buildings of research institutes and motorways. A DJI Phantom 4 Pro unmanned aerial vehicle flew up to an altitude of 30.7 m and approached an automated weather station, mounted at a mast near the Observatory. Time series of turbulent fluctuations of the longitudinal and transverse components of the horizontal wind were received with the use of the automated weather station, and time series of turbulent fluctuations of estimates of these components, from data of unmanned aerial vehicle in the hovering mode. According to the automated weather station, anisotropic fluctuations of the turbulent flow velocity were observed during the atmospheric measurements: the spectra of fluctuations of the horizontal components coincide, but differ from the spectrum of vertical fluctuations. The spectra of fluctuations of the longitudinal and transverse components of the horizontal wind velocity were comparatively analyzed. The general coincidence of these spectra with the spectra of fluctuations of estimates of the components is shown, with, however, significant differences in the high-frequency spectral region.

Keywords: unmanned aerial vehicle, urban atmospheric turbulence, spectrum, fluctuations, low-altitude sounding.

1. INTRODUCTION

Techniques for remote sounding of atmospheric turbulence with the use of unmanned aerial vehicles are of great interest in a wide range of scientific and applied problems, such as control of unmanned vehicles of a "smart city", study of changes in the urban climate, monitoring of air pollution in urban environment, forests, canyons, and other regions with complex orography.

The results of sounding of wind velocity in the lower atmosphere with unmanned aerial multirotor vehicles are presented in [1–5]. The wind velocity and direction in these works are determined by direct and indirect techniques. In the direct techniques, a 2D acoustic anemometer was mounted at a high carrying capacity hexacopter. In the indirect technique, the wind velocity and direction were estimated on the basis of data on the quadcopter state. The wind velocity is estimated both during hovering and vertical flight of the quadcopter. The wind velocity and direction techniques were validated with the use of sodars and acoustic anemometers. The studies have shown the equal wind velocity accuracy in the direct and indirect techniques and higher wind direction accuracy in the indirect technique.

The correlation tensor of wind velocity fluctuations and the related longitudinal and transverse components of wind velocity fluctuations and their spectra are important characteristics of the wind velocity field in a turbulent atmosphere [6, 7]. Therefore, the results of the study of estimation of the longitudinal and transverse components of wind velocity fluctuations with the use of unmanned aerial vehicles can form the scientific basis for low-altitude sounding of turbulence in the urban atmosphere.

The longitudinal and transverse components of wind velocity fluctuations are estimated in [8] with the use of a DJI Phantom 4 Pro quadcopter with special selection of the experimental conditions. During the experiments in the

* ash@imces.ru

Remote Sensing Technologies and Applications in Urban Environments V, edited by Thilo Erbertseder, Nektarios Chrysoulakis, Ying Zhang, Proc. of SPIE Vol. 11535, 1153506 · © 2020 SPIE
CCC code: 0277-786X/20/$21 · doi: 10.1117/12.2573486

Geophysical Observatory of IMCES SB RAS in Tomsk Akademgorodok, a quadcopter was northward oriented when hovering; a southern wind was actually observed. Under those conditions, fluctuations of the pitch and yaw angles during hovering are proportional to the estimates of fluctuations of the longitudinal and transverse components of horizontal wind velocity.

The aim of this work is, first, the derivation of equations for estimation of turbulent fluctuations of the longitudinal and transverse components of horizontal wind velocity independently of quadcopter orientation and wind direction. The second aim is the comparative analysis of the spectra of fluctuations of these wind velocity components recorded with the use of AMK-03 automated weather station and the spectra of fluctuations of estimates of these components recorded with a hovering DJI Phantom 4 Pro quadcopter. The experiment was carried out at the Geophysical Observatory of IMCES SB RAS, i.e., over the complex orography region, like in [8].

2. WIND VELOCITY ESTIMATION

Dynamic equations for the center of gravity of a quadcopter can be written in an inertial coordinates associated with the Earth as

$$\ddot{x} = \left(s_\varphi s_\psi + c_\varphi s_\theta c_\psi\right)\frac{T}{m} + \frac{F_x}{m}, \tag{1}$$

$$\ddot{y} = \left(-s_\varphi c_\psi + c_\varphi s_\theta s_\psi\right)\frac{T}{m} + \frac{F_y}{m}, \tag{2}$$

$$\ddot{z} = c_\varphi c_\theta \frac{T}{m} - g + \frac{F_z}{m}, \tag{3}$$

where $s_{(\bullet)} = \sin(\bullet)$, $c_{(\bullet)} = \cos(\bullet)$; φ is the roll angle; θ is the pitch angle; ψ is the yaw angle; T is the aerodynamic force generated by propellers; F_x, F_y, and F_z are the drag force components along the *x*, *y*, and *z* axes; m is the quadcopter mass; g is the gravity acceleration.

The components of the drag force along the *x*, *y*, and *z* axes, which arise during a quadcopter flight have the form:

$$F_j = -c_j\left(v_j - w_j\right) \tag{4}$$

in the linear case and

$$F_j = -\frac{1}{2}\rho C_j A_j \operatorname{sgn}\left(v_j - w_j\right) \times \left(v_j - w_j\right)^2 \tag{5}$$

in the square-law case. In Eqs. (4) and (5), c_j and C_j are the drag indices along the *x*, *y*, and *z* axes; j is the subscript for enumeration of the orthogonal components of vectors, i.e., $j \in \{x, y, z\}$; v_j are the quadcopter velocity components, and w_j are the velocity components of a turbulent flow in the atmosphere ; ρ is the air density; A_j are the projections of the quadcopter area on the corresponding axes; $\operatorname{sgn}(\bullet)$ is the sign function.

Based on dynamic equations for quadcopter center of gravity (1)–(3), the equation for estimates of the horizontal wind components for ideal hovering of a northward oriented unmanned aerial vehicle $\psi \approx 0$ and southern or northern winds were derived in [8]. Let us consider an ideal hover of an arbitrary oriented ($\psi \neq 0$) unmanned aerial vehicle. It is well known that ideal hovering is when all forces which act on a quadcopter are compensated at $v_j = 0$. If $\ddot{x} = \ddot{y} = \ddot{z} = 0$ and $v_j = 0$, the equations for estimates of horizontal components of turbulent flow velocity take the following form after required transformations:

$$\hat{w}_x = -\frac{mg}{c_x}\left(\langle\varphi\rangle s_{\langle\psi\rangle} + \langle\theta\rangle c_{\langle\psi\rangle}\right) - \frac{mg}{c_x}\left(\varphi' s_{\langle\psi\rangle} + \theta' c_{\langle\psi\rangle}\right), \tag{6}$$

$$\hat{w}_y = -\frac{mg}{c_y}\left(-\langle\varphi\rangle c_{\langle\psi\rangle} + \langle\theta\rangle s_{\langle\psi\rangle}\right) - \frac{mg}{c_y}\left(-\varphi' c_{\langle\psi\rangle} + \theta' s_{\langle\psi\rangle}\right) \tag{7}$$

in the linear case and

$$\hat{w}_x = -\mathrm{sgn}\left(\langle\varphi\rangle s_{\langle\psi\rangle} + \langle\theta\rangle c_{\langle\psi\rangle}\right)\sqrt{\frac{2mg}{\rho C_x A_x}\left|\langle\varphi\rangle s_{\langle\psi\rangle} + \langle\theta\rangle c_{\langle\psi\rangle}\right|}\left\{1 + \frac{\varphi' s_{\langle\psi\rangle} + \theta' c_{\langle\psi\rangle}}{2\left(\langle\varphi\rangle s_{\langle\psi\rangle} + \langle\theta\rangle c_{\langle\psi\rangle}\right)}\right\}, \tag{8}$$

$$\hat{w}_y = -\mathrm{sgn}\left(-\langle\varphi\rangle c_{\langle\psi\rangle} + \langle\theta\rangle s_{\langle\psi\rangle}\right)\sqrt{\frac{2mg}{\rho C_y A_y}\left|-\langle\varphi\rangle c_{\langle\psi\rangle} + \langle\theta\rangle s_{\langle\psi\rangle}\right|}\left(1 + \frac{-\varphi' c_{\langle\psi\rangle} + \theta' s_{\langle\psi\rangle}}{2\left(-\langle\varphi\rangle c_{\langle\psi\rangle} + \langle\theta\rangle s_{\langle\psi\rangle}\right)}\right) \tag{9}$$

in the square-law case. Equations (6)–(9) imply that the estimates of the horizontal components of turbulent flow velocity are the sum of the regular and fluctuation parts regardless of the drag model. The regular part of the estimates is determined by the average values of the $\langle\varphi\rangle$ and $\langle\theta\rangle$ angles, and the fluctuation part is proportional to the fluctuations of the roll and pitch angles.

3. MODEL OF ATMOSPHERIC TURBULENCE

An airflow in the atmosphere is accompanied by random temporal and spatial fluctuations. Therefore, the turbulent flow velocity is represented as the sun of the mean and fluctuation parts [6, 7]:

$$\mathbf{w}(\mathbf{r},t) = \langle\mathbf{w}(\mathbf{r},t)\rangle + \mathbf{w}'(\mathbf{r},t), \tag{10}$$

where

$$\langle\mathbf{w}(\mathbf{r},t)\rangle = \left\{\langle w_X(\mathbf{r},t)\rangle, \langle w_Y(\mathbf{r},t)\rangle, \langle w_Z(\mathbf{r},t)\rangle\right\} \tag{11}$$

is the mean velocity,

$$\mathbf{w}'(\mathbf{r},t) = \left\{w'_X(\mathbf{r},t), w'_Y(\mathbf{r},t), w'_Z(\mathbf{r},t)\right\}, \tag{12}$$

are the fluctuations of the turbulent flow velocity, $\langle w_p(\mathbf{r},t)\rangle$ and $w'_p(\mathbf{r},t)$ are the orthogonal mean and fluctuation components of wind velocity defined in the $\{\mathrm{X},\mathrm{Y},\mathrm{Z}\}$ coordinates, $p = \{\mathrm{X},\mathrm{Y},\mathrm{Z}\}$, $\langle\ldots\rangle$ is the operator of statistical averaging. We use the coordinates commonly accepted in meteorology [7]: the X axis is eastward directed (E), the Y axis is northward directed (N), and the Z axis is upward directed and is normal to the actual horizon surface.

When mathematically describing the wind velocity fluctuations under an isotropic turbulence, the longitudinal component

$$B_{rr}(r) = n_p n_q B_{pq}(r) \tag{13}$$

and the transverse component

$$B_{tt}(r) = \frac{1}{2}\left(\delta_{pq} - n_p n_q\right)B_{pq}(r) \tag{14}$$

of the correlation tensor are introduced [6, 7]. Here, $B_{pq}(r) = \langle w'_p(\mathbf{r}',t) w'_q(\mathbf{r}'+\mathbf{r},t)\rangle$ is the second-rank correlation tensor, $\mathbf{n} = \{n_q\} = \frac{\mathbf{r}}{r}$, $r = |\mathbf{r}|$. Summation is carried out over double subscripts in Eqs. (13) and (14).

If horizontal air mass transfer prevails over vertical movement, then the vector direction in Eqs. (13) and (14) should be chosen as the mean horizontal wind direction, i.e.,

$$\mathbf{n} = \{n_X, n_Y, 0\} = \left\{ \frac{\langle w_X \rangle}{\langle w_{\|} \rangle}, \frac{\langle w_Y \rangle}{\langle w_{\|} \rangle}, 0 \right\}, \tag{15}$$

where $\langle w_X \rangle$ and $\langle w_Y \rangle$ are the horizontal wind velocity components along the X and Y axes; $w_{\|} = \sqrt{\langle w_{\|X} \rangle^2 + \langle w_{\|Y} \rangle^2}$ is the horizontal wind velocity.

Substituting Eq. (15) in Eqs. (13) and (14), we derive

$$B_{rr}(r) = \langle w'_r(\mathbf{r}_1, t) w'_r(\mathbf{r}_1 + \mathbf{r}, t) \rangle, \tag{16}$$

$$B_{tt}(r) = \langle w'_t(\mathbf{r}_1, t) w'_t(\mathbf{r}_1 + \mathbf{r}, t) \rangle + \langle w'_{\perp}(\mathbf{r}_1, t) w'_{\perp}(\mathbf{r}_1 + \mathbf{r}, t) \rangle. \tag{17}$$

Here,

$$w'_r(\mathbf{r}, t) = n_X w'_X(\mathbf{r}, t) + n_Y w'_Y(\mathbf{r}, t) \tag{18}$$

is the longitudinal component of wind velocity fluctuations, and

$$w'_t(\mathbf{r}, t) = -n_Y w'_X(\mathbf{r}, t) + n_X w'_Y(\mathbf{r}, t), \tag{19}$$

$$w'_{\perp}(\mathbf{r}, t) = w'_Z(\mathbf{r}, t). \tag{20}$$

are two transverse components; component (19) is in the horizontal XOY plane, and component (20) is directed along the Z axis.

For isotropic fluctuations of the turbulent flow velocity field in the inertial range of wavenumbers, the Kolmogorov–Obukhov "5/3" law is fulfilled [7]. For the spectral density of the average kinetic energy of unit air mass, it has the form

$$E(k) \sim \varepsilon \cdot k^{-5/3}, \tag{21}$$

where ε is the dissipation rate of turbulent kinetic energy.

Based on the Taylor hypothesis about "frozen" turbulent fluctuations, the equation which connects the frequency spectrum of a random field with its spatial spectrum was derived in [7]. Using this relationship, one can write an equation for the frequency spectrum in the case of the Kolmogorov–Obukhov "5/3" law [7]:

$$\Phi(f) \sim f^{-5/3}. \tag{22}$$

According to Eq. (22), the frequency spectrum of a random wind velocity field damps proportional to the frequency in the power –5/3.

4. ESTIMATES OF LONGITUDINAL AND TRANSVERSE COMPONENTS

Let us estimate the longitudinal and transverse components of wind velocity fluctuations by analogy with Eqs. (18) and (19) as

$$\hat{w}'_r(\mathbf{r}, t) = \hat{n}_x \hat{w}'_x(\mathbf{r}, t) + \hat{n}_y \hat{w}'_y(\mathbf{r}, t), \tag{23}$$

$$\hat{w}'_t(\mathbf{r}, t) = -\hat{n}_x \hat{w}'_y(\mathbf{r}, t) + \hat{n}_y \hat{w}'_x(\mathbf{r}, t), \tag{24}$$

where $\hat{w}'_r(\mathbf{r}, t)$ is the estimate of the longitudinal component, and $\hat{w}'_t(\mathbf{r}, t)$, of the transverse component in the xOy plane. The direction of the vector $\mathbf{n}$ in Eqs. (23) and (24) can be estimated by the equation

$$\hat{\mathbf{n}} = \{\hat{n}_x, \hat{n}_y, 0\} = \left\{ \frac{\langle \hat{w}_x \rangle}{\langle \hat{w}_{\|} \rangle}, \frac{\langle \hat{w}_y \rangle}{\langle \hat{w}_{\|} \rangle}, 0 \right\}, \tag{25}$$

where $\langle \hat{w}_x \rangle$ and $\langle \hat{w}_y \rangle$ are the estimates of the components of the horizontal wind velocity along the x and y axes; $\hat{w}_{\|} = \sqrt{\langle \hat{w}_x \rangle^2 + \langle \hat{w}_y \rangle^2}$ is the estimate of the horizontal wind velocity.

5. GENERAL INFORMATION ABOUT EXPERIMENT

Experimental studies were carried out on the basis of the Geophysical Observatory of IMCES SB RAS. It is situated in Tomsk Akademgorodok, on the territory with complex orography, in a parkland zone with buildings of research institutes and motorways. The experiment took place on February 26, 2020, from 10:06 to 10:27 UTC.

Figure 1 shows the quadcopter flight trajectory during the experiment. A DJI Phantom 4 Pro drone was launched in close proximity to the Observatory building. After takeoff, it climbed to an altitude of 30.7 m and flew up to AMK-03 automated weather station, which was mounted at a mast in the immediate vicinity of the Observatory. The quadcopter axis *x* was northward oriented. The quadcopter hold the altitude near AMK-03 for more than 15 min and then returned to the starting point.

The AMK-03 automated weather station is designed to measure and record wind velocity and direction, air temperature and relative humidity, and atmospheric pressure. The wind data were recorded at a frequency of 80 Hz. The quadcopter state (time series of the roll, pitch, and yaw angles) was recorded with a frequency of 10 Hz. When calculating the spectra of wind velocity fluctuations, the AMK-03 data were reduced to a frequency of 10 Hz.

According to data of the Tomsk International Airport, which is located at a distance of ~10 km from the building of the Geophysical Observatory of IMCES SB RAS, the weather conditions were difficult for quadcopter flight during the experiment: southern wind at a velocity of 2–3 m/s, air temperature of –5°C, and air humidity of 69%.

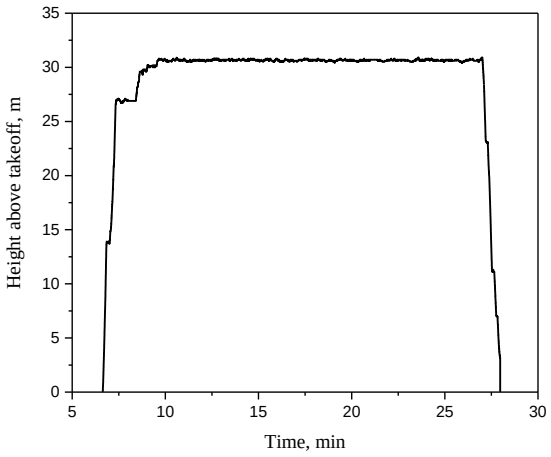

Figure 1. Quadcopter flight trajectory during the experiment.

6. MEASUREMENT RESULTS

Figure 2 shows variations in the quadcopter velocity components along the *x*, *y*, and *z* axes during hovering. The quadcopter velocity components were generally zero during the measurements. Sometimes, the forces which acted on the quadcopter exceeded the capabilities of the control system for a short time, and high-precision positioning was perturbed. After control recovery, the quadcopter began moving to its original position and stopped upon reaching it. Thus, the time periods when the spatial positioning of the quadcopter was perturbed can be ignored due to their insignificance, and the hover could be considered ideal during the experiment.

The experimental study of the atmospheric turbulence effect on the operation of a DJI Phantom 4 Pro quadcopter, carried out on February 20, 2020, from 10:21 to 10:34 UTC, is described in [8]. That experimental site was the same, but the weather conditions were more severe: south-southwest wind with a velocity 6.0 m/s, air temperature of –1.5°C, air

humidity of 100%, and snowing. The comparison between the data in Figure 2 with the results [8] shows that more severe weather conditions result in a stronger deviation from ideal hovering.

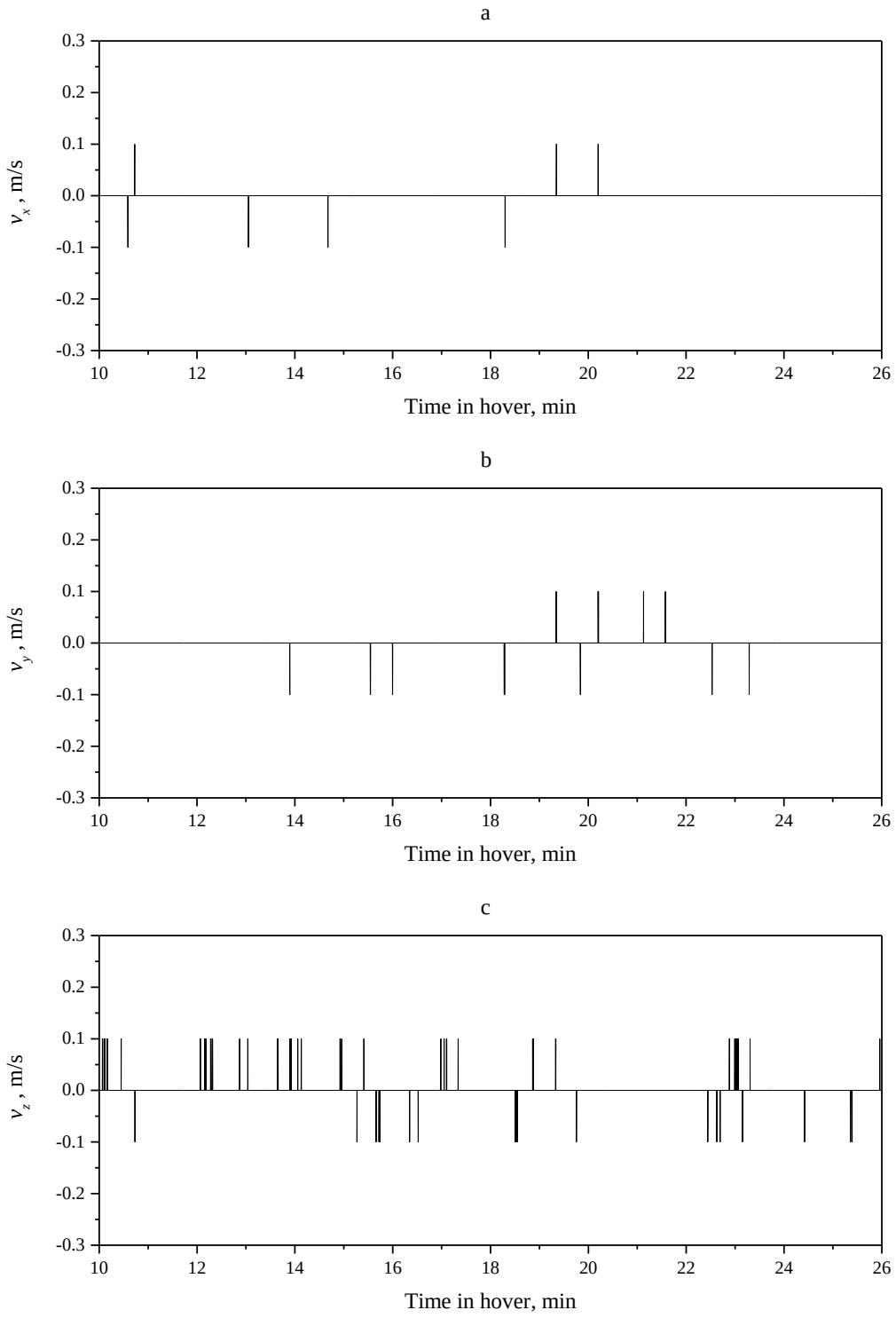

Figure 2. Quadcopter velocity components along the (a) *x*, (b) *y*), and (c) *z* axes during hovering.

Let us consider the behavior of the estimates of the longitudinal $\hat{w}_r(\mathbf{r},t)$ and transverse $\hat{w}_t(\mathbf{r},t)$ components of wind velocity in a turbulent atmosphere in the altitude holding mode. Figure 3 shows the time series of these estimates (black curve) and of the longitudinal $w_r(\mathbf{r},t)$ and transverse $w_t(\mathbf{r},t)$ components of wind velocity (red curve) measured by AMK-03 automated weather station. The $\hat{w}_r(\mathbf{r},t)$ and $\hat{w}_t(\mathbf{r},t)$ time series are normalized with the use of their maximal and minimal values and the average $w_r(\mathbf{r},t)$ and $w_t(\mathbf{r},t)$ values. It follows from Fig. 3 that the wind velocity components and their estimates generally coincide, and the differences are observed in the region of high-frequency fluctuations. Similar behavior of the estimates of the wind velocity components along the *x*, *y*, and *z* axes was observed in the experiment [8].

For objective assessment of the spectra of fluctuations of the longitudinal and transverse components of the wind velocity and their estimates, 13.65-min averaging was applied. The spectra were calculated with the use of standard FFT algorithms and a smoothing procedure. Figure 4 shows relative fluctuation spectra of the longitudinal and transverse wind velocity components calculated on the basis of AMK-03 data, and relative fluctuation spectra of the estimates of the longitudinal and transverse wind velocity components calculated from DJI Phantom 4 Pro quadcopter telemetry data. The dashed line in Fig. 4 shows the fluctuation power spectrum $\Phi(f) \sim f^{-5/3}$, which corresponds to the Kolmogorov–Obukhov "5/3" law; σ^2 is the normalization coefficient.

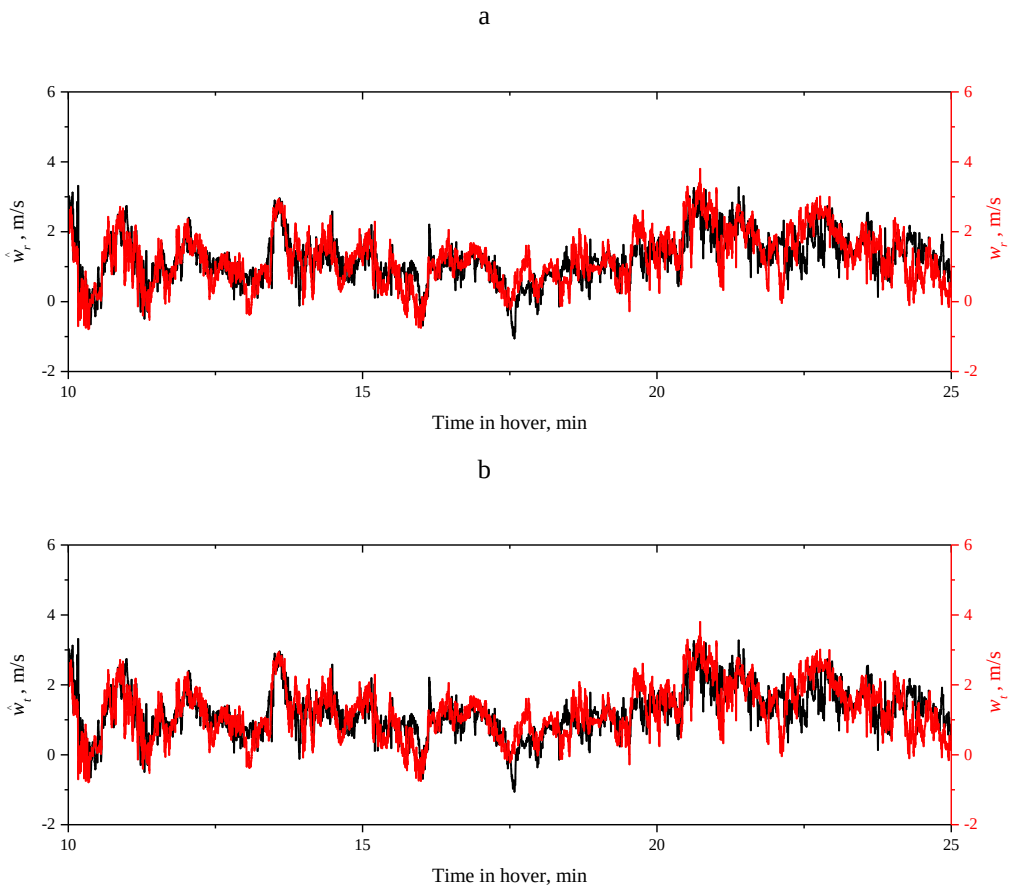

Figure 3. Temporal variations in the (a) estimates of the longitudinal $\hat{w}_r$ and transverse $\hat{w}_t$ components of the horizontal wind velocity (black curve); (b) in the longitudinal w_r and transverse w_t wind velocity components during hovering (red curve).

Figure 4a shows anisotropy of wind velocity fluctuations during AMK-03 measurements: the fluctuation spectra of the w'_r and w'_t components coincide, but differ from the spectrum of vertical fluctuations $w'_\perp = u'_Z$. It also shows coincidence of the spectra of fluctuations of the w_r and w_t components with the Kolmogorov–Obukhov "5/3" spectrum in a wide frequency range. As follows from Fig. 4b, the fluctuation spectra of estimates of the transverse $\hat{w}'_r$ and longitudinal components $\hat{w}'_t$ coincide. In addition, the spectra damp with an increase in the frequency proportional to the power –5/3, i.e., they coincide with the Kolmogorov–Obukhov "5/3" spectrum, in a wide frequency range.

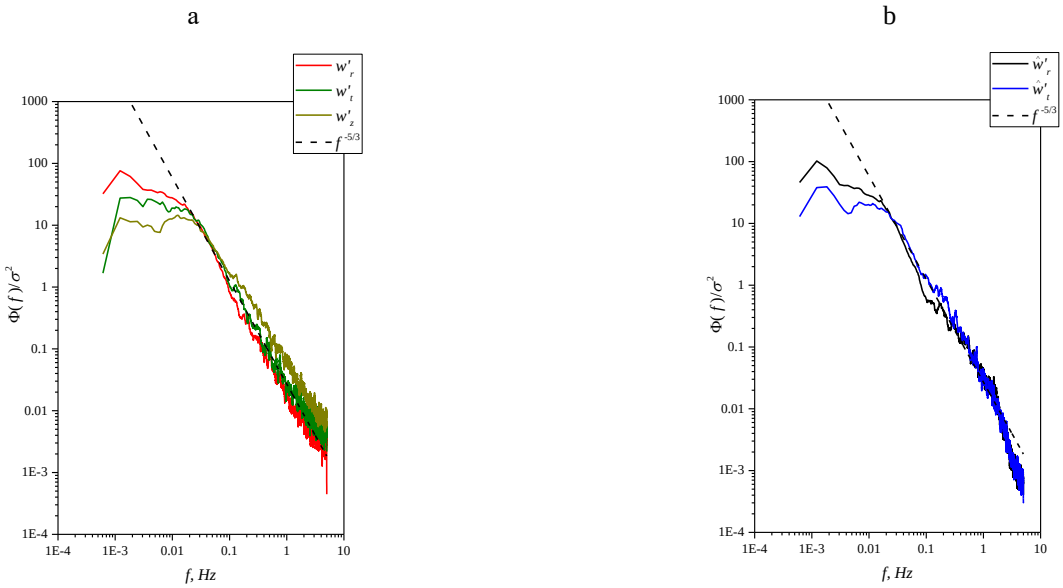

Figure 4. Spectra of fluctuations of the (a) longitudinal w'_r and transverse w'_t components of the horizontal wind velocity and (b) estimates of the longitudinal $\hat{w}'_r$ and transverse $\hat{w}'_t$ components of the horizontal wind velocity

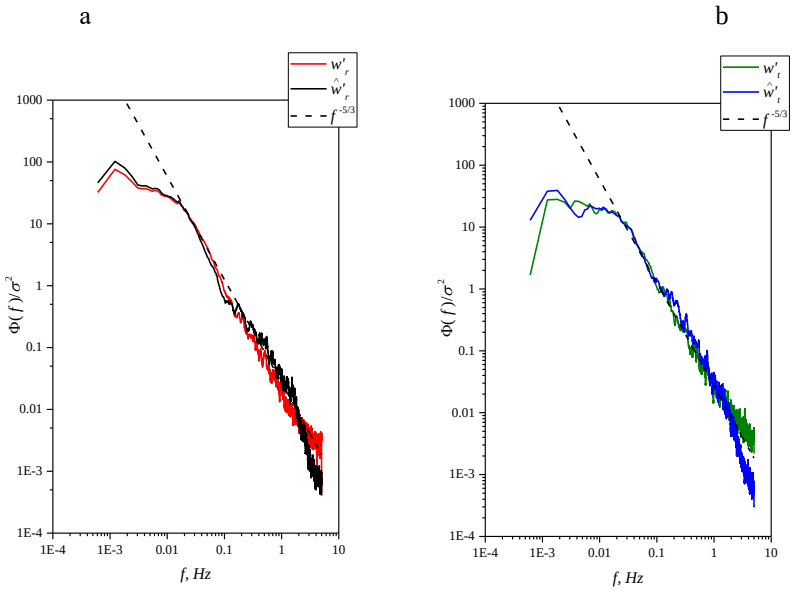

Figure 5. Comparison between the fluctuation spectra of the (a) longitudinal wind velocity component w'_r and its estimate $\hat{w}'_r$; (b) transverse wind velocity component w'_t and its estimate $\hat{w}'_t$

Figure 5 shows the results of comparison between the spectra of fluctuations of the transverse and longitudinal wind velocity components and the spectra of fluctuations of their estimates. The dashed line in Fig. 5 shows the fluctuation power spectrum, which corresponds to the Kolmogorov-Obukhov "5/3" law, and the normalization coefficient. One can see that the fluctuation spectra of the transverse and longitudinal wind velocity components and the fluctuation spectra of their estimates generally coincide, but significant differences are observed in the high-frequency spectral region.

7. ACKNOWLEDGMENTS

The reported study was funded by RFBR, project number 19-29-06066 mk.

REFERENCES

[1] Palomaki, R. T., Rose, N. T., van den Bossche, M., Sherman, T. J., and De Wekker, S. F. J., "Wind estimation in the lower atmosphere using multirotor aircraft," J. Atmos. Ocean. Technol. 34, 1183–1190 (2017). DOI: 10.1175/JTECH-D-16-0177.1
[2] Neumann, P. P. and Bartholmai, M., "Real-time wind estimation on a micro unmanned aerial vehicle using its internal measurement unit," Sens. Actuators 235A, 300–310 (2015). DOI:10.1016/j.sna.2015.09.036.
[3] González-Rocha, J., De Wekker, S. F. J., Ross, S. D., and Woolsey, C. A., "Wind Profiling in the lower atmosphere from wind-induced perturbations to multirotor," UAS. Sensors 20, 1341 (2020).
[4] González-Rocha, and Woolsey, C. A., "Cornel Sultan measuring atmospheric winds from quadcopter motion," AIAA Atmospheric Flight Mechanics Conference. 9–13 January 2017, Grapevine, Texas. DOI: 10.2514/6.2017-1189.
[5] Allison, S.; Bai, H.; Jayaraman, B. Wind estimation using quadcopter motion: A machine learning approach. Aerosp. Sci. Technol. 2020, 98, 105699.
[6] Stull, R.B. [An Introduction to Boundary Layer Meteorology], Kluwer Academic Publishers, Netherlands (1989).
[7] Monin, A. S. And Yaglom, A. M. [Statistical Hydromechanics. Part 2. Turbulent Mechanics], Nauka, Moscow, (1967).
[8] Shelekhov A.P, Afanasiev A.L., Kobzev A.A., Chupina O.S., Tel'minov A.E., Shelekhova E.A. Spectra of turbulent fluctuations of Euler angles of unmanned aerial vehicles in the altitude holding mode. // Proc. SPIE International Symposium on Atmospheric and Ocean Optics, Atmospheric Physics (AOO20). 2020. In print.